Zhang *et al.*
Chinese Journal of Mechanical Engineering (2024) 37:78
https://doi.org/10.1186/s10033-024-01050-4

Chinese Journal of Mechanical Engineering

ORIGINAL ARTICLE

Open Access

Dynamic Modeling and Experimental Verification of an RPR Type Compliant Parallel Mechanism with Low Orders

Shuang Zhang[1], Jingfang Liu[2,3*], Huafeng Ding[2,4] and Yanbin Zhang[1,5]

Abstract

Efficiency of calculating a dynamic response is an important point of the compliant mechanism for posture adjustment. Dynamic modeling with low orders of a 2R1T compliant parallel mechanism is studied in the paper. The mechanism with two out-of-plane rotational and one lifting degrees of freedom (DoFs) plays an important role in posture adjustment. Based on elastic beam theory, the stiffness matrix and mass matrix of the beam element are established where the moment of inertia is considered. To improve solving efficiency, a dynamic model with low orders of the mechanism is established based on a modified modal synthesis method. Firstly, each branch of the RPR type mechanism is divided into a substructure. Subsequently, a set of hypothetical modes of each substructure is obtained based on the C-B method. Finally, dynamic equation of the whole mechanism is established by the substructure assembly. A dynamic experiment is conducted to verify the dynamic characteristics of the compliant mechanism.

Keywords Compliant parallel mechanism, Dynamic model, Modal synthesis method, Dynamic experiment

1 Introduction

In recent decades, the flexure-hinge-based compliant mechanism has attracted widespread attention from a variety of applications in miniature and nanometer technology. Due to its no friction, no backlash, easy to miniaturization and other advantages, the flexure-hinge-based compliant mechanism with out-of-plane rotation DoFs has important value in applications for posture-adjustment, such as cell operation [1, 2], micro- or nano-machining [3–5] and wafer alignment in microlithography [6].

To date, a variety of compliant mechanisms with out-of-plane rotation DoFs have been proposed and studied for diverse applications. He et al. [7] presented a novel compact single-mirror laser scanner based on a 3-PRS compliant mechanism actuated by the permanent magnetic suspension. Kim et al. [8] designed and modeled a precision micro-stage based on the well-known tripod parallel configuration for active micro-vibration control. Park and Lee [9] proposed a piezoelectric-driven tilt mirror for a fast laser scanner. Kim et al. [10] developed a nano-precision 2R1T vertical positioning stage which can compensate for the deformation caused by gravity. Hao et al. [11] also proposed a 2R1T compliant mechanism based on the constraint-based design method. Yu et al. [12] proposed a 2R1T compliant parallel mechanism for optical fiber alignment. In our previous work, an RPR type 2R1T compliant parallel mechanism was proposed [13]. The RPR type mechanism has two vertical

*Correspondence:
Jingfang Liu
jfliu@bjut.edu.cn
[1] School of Mechatronics Engineering, Henan University of Science and Technology, Luoyang, Henan, China
[2] Faculty of Materials and Manufacturing, College of Mechanical Engineering and Applied Electronics Technology, Beijing University of Technology, Beijing, China
[3] Key laboratory of advanced manufacturing technology, Beijing University of Technology, Beijing, China
[4] School of Mechanical Engineering and Electronic Information, China University of Geosciences (Wuhan), Wuhan, China
[5] Center of Machinery Equipment Advanced Manufacturing of Henan Province, Luoyang, China

continuous rotation axes relative to the fixed coordinate, which are known. One of them is fixed to the fixed platform; the other one is close to the moving platform, and its position and direction change in motion. Due to its kinematic characteristics, the RPR type mechanism has the advantages of easy control and high orientation accuracy.

More compliant mechanism applications have been extended to address high speed and high frequency. Thus, dynamic modeling has become an urgent research task. This can be crucial for evaluating or optimizing dynamic performance and for designing controllers. The pseudo rigid body model method (PRBMM) [14–16] is a versatile tool that can be used for static and dynamic modeling and analysis of compliant mechanisms. The dynamic model can be established by calculating the kinematics with characteristic parameters based on the Lagrange dynamic modeling approach. Similar to the PRBMM, kinematic DOFs of compliant mechanisms are usually taken as variables in a lumped-parameter dynamic model [17, 18]. However, this method is mostly used for small deformation mechanisms with low accuracy. In the distributed-parameter model [19, 20], elastic deformations of each flexure member or rigid-body member are taken as the variables. The dynamic model is established by formulating the total elastic and kinetic energies and combining them with Lagrange's equation. Because more degrees of freedom are considered, accuracy of the distributed parameter method is usually higher than that of the lumped-parameter dynamic model, yet the order of the dynamic model is larger. The transfer matrix method [21] has the advantages of low equation order and easy programming. However, the method is rarely applied for spatial compliance mechanisms due to complex structures. Recently, Ling et al. [22–26] proposed a dynamic stiffness modeling method based on D'Alembert's principle for simultaneous kinetostatics and dynamic model of compliant mechanisms with small deflection in a static manner. However, the element dynamic stiffness matrix needs to be obtained in advance. In linear elasticity theory, the dynamics of spring-mass systems have been extensively studied. A variety of dynamic methods have been proposed and applied to complex structures, such as the reverberation ray matrix method [27, 28] and spectral element method [29]. These methods can be effectively used in the dynamic modeling and analysis of complex structures (such as trusses). However, they are not currently used in compliant mechanisms.

The dynamic control of compliant mechanisms requires the establishment of a dynamic model with high accuracy in solving dynamic responses and high computational efficiency. Therefore, based on the distributed-parameter model method, a dynamic model with low orders of an RPR type mechanism is established for future application in the paper. The modal synthesis method is modified for dynamic modeling of compliant mechanisms for the first time. The remainder of this paper is organized as follows. A brief introduction of the modal synthesis method is given in Section 2. The elastic element modeling is established in Section 3. In Section 4, a dynamic modeling with low orders of the whole RPR type mechanism is established. Simulations and experiments are carried out to verify the analytical modeling in Sections 5 and 6, respectively. Finally, a conclusion is given in Section 7.

2 Application of the Modal Synthesis Method in Compliant Parallel Mechanisms

For a complex spring-mass system, a dynamic solution meeting the accuracy requirements over a short time is of great significance for real-time control. Due to complex structure, the dynamic model of the spatial parallel compliant mechanism is considerably cumbersome. Improving the efficiency of the dynamic calculation is one of the keys to practical application of this kind of mechanism.

The modal synthesis method is an efficient way to reduce the order of dynamic model and improve the efficiency of dynamic calculation. The basic concept of the method is that the order of the overall dynamic equation of the mechanism is reduced by discarding higher-order modes of substructures in a complex spring-mass system. The core of the modal synthesis method is to obtain a set of high-quality hypothetical modals. The hypothetical modes, as the modal space expanded by the Ritz basis, can well cover the actual low-order modal space of the system. Therefore, the modal synthesis method can not only simplify the calculation of the dynamic characteristics of complex mechanisms, but also simplify the calculation of the dynamic response.

The steps of the modal synthesis method of the compliant parallel mechanism can be summarized as follows:

1. According to the structural characteristics, branches of the compliant parallel mechanism are split as substructures.

2. Based on the mechanical analysis, a set of hypothetical modes with a higher quality of each substructure is constructed.

3. The physical coordinates of each substructure are transformed into modal coordinates according to the set of hypothetical modes.

4. Through the interface connection conditions, the dependent modal coordinates are eliminated. Then, the dynamic equation represented by the independent modal coordinates of the whole system is derived.

5. According to the obtained modal matrix, the modal coordinates are transformed into physical coordinates to reproduce the physical state of the system.

Craig and Bampton [30] improved the fixed interface modal synthesis method proposed by Hurty [31], which is called the C-B method. In the C-B method, the hypothetical mode is constructed based on the kinematics of the substructure. The hypothetical modal set obtained by the C-B method has two subsets, i.e., the reserved main modal set with all interfaces fixed and the constrained modal set containing all interface coordinates. The displacement of any point in the substructure can be described by these two modal sets. Because of intuitiveness and practicability, the C-B method is modified and used here for the RPR type compliant mechanism.

The hypothetical modal set can be expressed as

$$[\boldsymbol{\psi}]^{\lambda} = \left[\left[\boldsymbol{\psi}_k\right]^{\lambda} \ \left[\boldsymbol{\psi}_c\right]^{\lambda} \right], \tag{1}$$

where $\left[\boldsymbol{\psi}_k\right]^{\lambda}$ is the reserved main modal set. $\left[\boldsymbol{\psi}_c\right]^{\lambda}$ is the constrained modal set.

After the interfaces are fixed, the main modal set can be obtained by solving the dynamic characteristic equation of the substructure.

$$\left(\left[\hat{\boldsymbol{K}}\right]^{\lambda} - \omega^2\left[\hat{\boldsymbol{M}}\right]^{\lambda}\right)\left\{\boldsymbol{\psi}_{ik}\right\} = \{\boldsymbol{0}\}. \tag{2}$$

Let $\left[\boldsymbol{\psi}_{ik}\right]$ be a part of the low-order modal set after truncating the high-order modes of $\left\{\boldsymbol{\psi}_{ik}\right\}$. The order of the reserved low-order main modal set $\left[\boldsymbol{\psi}_{ik}\right]$ is smaller than that of the other set in $\left\{\boldsymbol{\psi}_{ik}\right\}$. The reserved main modal set of the substructure can be expressed as

$$\left[\boldsymbol{\psi}_k\right]^{\lambda} = \begin{bmatrix} \left[\boldsymbol{\psi}_{ik}\right] \\ \boldsymbol{0}_{ic} \end{bmatrix}, \tag{3}$$

where $\boldsymbol{0}_{ic}$ represents the mode of the fixed interface.

The function of the compliant parallel mechanism is to realize the transmission and conversion of force and motion. The main mode of the substructure can not reflect the actual motion of the compliant parallel mechanism, because the mode of its interface is 0. Therefore, the main modes of the substructure are all removed in the paper. In addition, the displacement of any point in the substructure can be expressed as the superposition of the elastic deformation of the substructure and the traction motion from the driving source. The motion in the compliant mechanism can be completely expressed by the constrained mode of the substructure.

For the constrained mode of the substructure, additional constraints are imposed on all the interface degrees of freedom. Then, the constrained interfaces are allowed to produce unit displacement along each degree of freedom in turn, while other constraints remain unchanged (The displacement of the constrained interface coordinate is forced to be 0). The resulting displacement of static deformation is called the constrained mode of the substructure. The number of constrained modes is equal to that of interface degrees of freedom. Hence, the constrained modal of the substructure can be expressed as

$$\left[\boldsymbol{\psi}_c\right]^{\lambda} = \begin{bmatrix} \boldsymbol{\psi}_{ic} \\ \boldsymbol{I}_{jc} \end{bmatrix}^{\lambda}, \tag{4}$$

where $\boldsymbol{I}_{jc}$ is an identity matrix. $\boldsymbol{\psi}_{ic}$ can be obtained by

$$\begin{bmatrix} \boldsymbol{k}_{ii} & \boldsymbol{k}_{ij} \\ \boldsymbol{k}_{ji} & \boldsymbol{k}_{jj} \end{bmatrix}^{\lambda} \begin{bmatrix} \boldsymbol{\psi}_{ic} \\ \boldsymbol{I}_{jc} \end{bmatrix}^{\lambda} = \begin{bmatrix} \boldsymbol{0}_{ic} \\ \boldsymbol{R}_{jc} \end{bmatrix}, \tag{5}$$

where $\begin{bmatrix} \boldsymbol{k}_{ii} & \boldsymbol{k}_{ij} \\ \boldsymbol{k}_{ji} & \boldsymbol{k}_{jj} \end{bmatrix}^{\lambda}$ is the stiffness matrix of the substructure. The meaning of $\boldsymbol{R}_{jc}$ is a constraint that makes boundary to produce unit displacements.

From Eq. (5), $\left[\boldsymbol{\psi}_c\right]^{\lambda}$ can be obtained by

$$\left[\boldsymbol{\psi}_c\right]^{\lambda} = \begin{bmatrix} \boldsymbol{\psi}_{ic} \\ \boldsymbol{I}_{jc} \end{bmatrix}^{\lambda} = \begin{bmatrix} -[\boldsymbol{k}_{ii}]^{-1}\left[\boldsymbol{k}_{ij}\right] \\ \boldsymbol{I}_{jc} \end{bmatrix}^{\lambda}. \tag{6}$$

Thus, the first coordinate transformation of the substructure can be expressed as

$$\{\boldsymbol{u}\} = \left[\boldsymbol{\psi}_c\right]^{\lambda}\{\boldsymbol{p}\}, \tag{7}$$

where $\{\boldsymbol{u}\}$ is the physical coordinate of the substructure representing the actual displacement of nodes in the substructure. $\{\boldsymbol{p}\}$ is the modal coordinate of the substructure.

3 Introduction of the RPR Type Mechanism and Stiffness Model of the Substructure

As shown in Figure 1, the RPR type compliant mechanism is driven by 4 piezoelectric actuators. And the branches are placed vertically and symmetrically. The topological structure of the mechanism is 2-UPR-2-RPU, which U represents the universal joint, R represents the revolute joint, and P represents the translational joint. The structures of the U pair and the R pair are shown in Figure 2, respectively. Their dimension parameters are given in Table 1. Distance from U pair to R pair in the same branch is equal to 40 mm. The distances from the

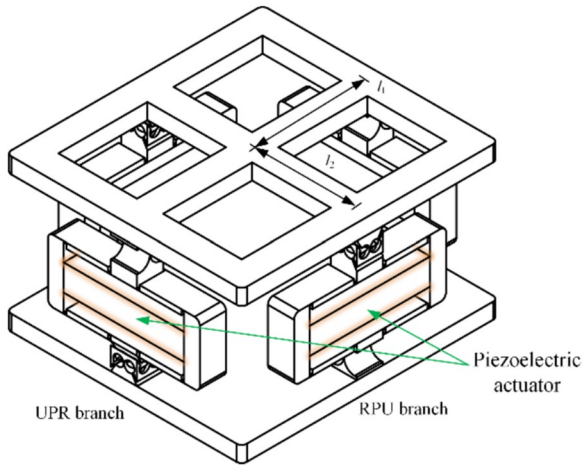

Figure 1 The RPR type compliant mechanism

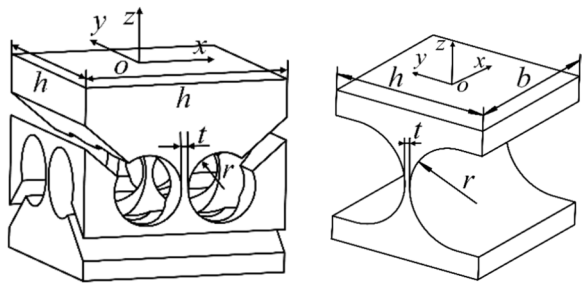

Figure 2 U complaint joint and R complaint joint

Table 1 Size parameters of flexible hinges

R pair (mm)	$R = 4$	$h = 10$	$b = 10$	t =0.03
U pair (mm)	$r = 1.5$	$h = 10$	$t = 0.03$	

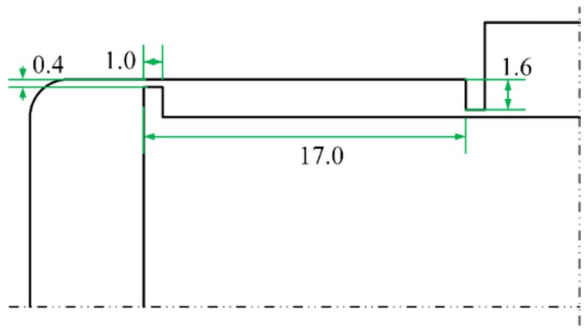

Figure 3 A quarter of the displacement amplifier

center point of the platform to the midpoint of the two branches are 40 mm and 48 mm, respectively. The translational joint is realized by bridge-type displacement amplifier, of which a quarter of the structure is shown in Figure 3. The displacement amplifier is installed close to the fixed platform.

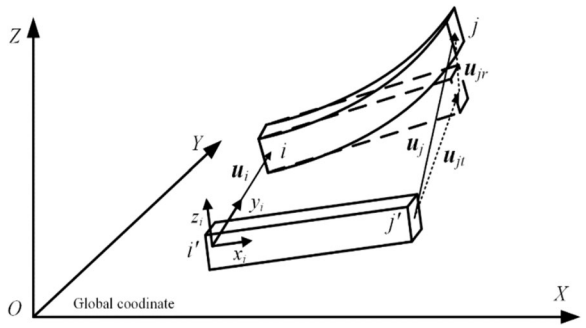

Figure 4 Schematic diagram of deformation of an elastic beam element

3.1 Mass Matrix and Stiffness Matrix of the Beam Element

In the paper, the flexure hinge and the connecting linkage of the RPR type compliant mechanism are regarded as elastic beam elements. For a beam element K, there are i and j nodes at its ends. The displacements of these two nodes can be expressed as

$$\boldsymbol{u}_i = \left(t_{ix} \;\; t_{iy} \;\; t_{iz} \;\; \alpha_{ix} \;\; \alpha_{iy} \;\; \alpha_{iz} \right)^{\mathrm{T}}, \tag{8}$$

$$\boldsymbol{u}_j = \left(t_{jx} \;\; t_{jy} \;\; t_{jz} \;\; \alpha_{jx} \;\; \alpha_{jy} \;\; \alpha_{jz} \right)^{\mathrm{T}}. \tag{9}$$

As shown in Figure 4, the displacement of node j includes the rigid motion of the bar with node i and the elastic deformation of the bar. The deformation of a point in the element can be expressed by the shape function

$$\Delta_k(x) = \boldsymbol{N}(x) \begin{bmatrix} \boldsymbol{u}_i \\ \boldsymbol{u}_j \end{bmatrix}, \tag{10}$$

where $\boldsymbol{N}(x)$ is the shape function matrix. The shape functions of the axial deformation and torsion deformation are determined as first-order polynomials, and those of the bending deformation are determined as third-order polynomials.

For the boundary conditions, the deformation at node i is 0, and the deformation at node j is

$$\Delta_k(j) = \left[-\boldsymbol{D}_k(j) \;\; \boldsymbol{I} \right], \tag{11}$$

where $\boldsymbol{D}_k(j) = \begin{bmatrix} \boldsymbol{E} & \hat{\boldsymbol{r}}_k(l_k) \\ \boldsymbol{0} & \boldsymbol{I} \end{bmatrix}$, $\boldsymbol{r}_k(j) = \left(0 \;\; 0 \;\; l_k \right)^{\mathrm{T}}$, and $\hat{\boldsymbol{r}}_k(l_k)$ is the skew-symmetric matrix defined by the translational vector $\boldsymbol{r}_k(l_k)$.

The shape function of the beam element can be obtained from the boundary condition.

$$\boldsymbol{N}(x)=\begin{bmatrix} -\frac{x}{l_k} & 0 & 0 & 0 & 0 & 0 & \frac{x}{l_k} & 0 & 0 & 0 & 0 & 0 \\ 0 & \frac{2x^3}{l_k^3}-\frac{3x^2}{l_k^2} & 0 & 0 & 0 & \frac{x^3}{l_k^2}-\frac{2x^2}{l_k} & 0 & \frac{3x^2}{l_k^2}-\frac{2x^3}{l_k^3} & 0 & 0 & 0 & \frac{x^3}{l_k^2}-\frac{x^2}{l_k} \\ 0 & 0 & \frac{2x^3}{l_k^3}-\frac{3x^2}{l_k^2} & 0 & -\frac{x^3}{l_k^2}+\frac{2x^2}{l_k} & 0 & 0 & 0 & \frac{3x^2}{l_k^2}-\frac{2x^3}{l_k^3} & 0 & -\frac{x^3}{l_k^2}+\frac{x^2}{l_k} & 0 \\ 0 & 0 & 0 & -\frac{x}{l_k} & 0 & 0 & 0 & 0 & 0 & \frac{x}{l_k} & 0 & 0 \\ 0 & 0 & -\frac{6x^2}{l_k^3}+\frac{6x}{l_k^2} & 0 & \frac{3x^2}{l_k^2}-\frac{4x}{l_k} & 0 & 0 & 0 & -\frac{6x}{l_k^2}+\frac{6x^2}{l_k^3} & 0 & \frac{3x^2}{l_k^2}-\frac{2x}{l_k} & 0 \\ 0 & \frac{6x^2}{l_k^3}-\frac{6x}{l_k^2} & 0 & 0 & 0 & \frac{3x^2}{l_k^2}-\frac{4x}{l_k} & 0 & \frac{6x}{l_k^2}-\frac{6x^2}{l_k^3} & 0 & 0 & 0 & \frac{3x^2}{l_k^2}-\frac{2x}{l_k} \end{bmatrix}. \quad (12)$$

The displacement of a point in the beam element is the sum of the motion caused by node i and the elastic deformation of the element, and can be expressed as

$$\boldsymbol{u}_k(x)=\overline{\boldsymbol{N}}_k\begin{bmatrix}\boldsymbol{u}_i\\ \boldsymbol{u}_j\end{bmatrix}, \quad (13)$$

where $\overline{\boldsymbol{N}}_k=\begin{bmatrix}\overline{\boldsymbol{N}}_{k1}\\ \overline{\boldsymbol{N}}_{k2}\end{bmatrix}=\left[\left(\boldsymbol{D}_k(x)\ \ \boldsymbol{0}\right)+\boldsymbol{N}(x)\right]$.

The kinetic energy of the element can be divided into translational kinetic energy and rotational kinetic energy. The translational kinetic energy is

$$T_{kt}=\frac{1}{2}\begin{bmatrix}\dot{\boldsymbol{u}}_i^{\mathrm{T}} & \dot{\boldsymbol{u}}_j^{\mathrm{T}}\end{bmatrix}\int_0^{l_k}\rho\overline{\boldsymbol{N}}_{k1}^{\mathrm{T}}A_k(x)\overline{\boldsymbol{N}}_{k1}\mathrm{d}x\begin{bmatrix}\dot{\mathbf{u}}_i\\ \dot{\boldsymbol{u}}_j\end{bmatrix}, \quad (14)$$

where $\dot{\boldsymbol{u}}_i$ and $\dot{\boldsymbol{u}}_j$ denote the velocities of nodes i and j, respectively.

The rotational kinetic energy is

$$T_{kr}=\frac{1}{2}\begin{bmatrix}\dot{\boldsymbol{u}}_i^{\mathrm{T}} & \dot{\boldsymbol{u}}_j^{\mathrm{T}}\end{bmatrix}\int_0^{l_k}\boldsymbol{N}_{k2}^{\mathrm{T}}\mathrm{d}\boldsymbol{I}\overline{\boldsymbol{N}}_{k2}\begin{bmatrix}\dot{\boldsymbol{u}}_i\\ \dot{\boldsymbol{u}}_j\end{bmatrix}, \quad (15)$$

where $\mathrm{d}\boldsymbol{I}=\begin{bmatrix}\mathrm{d}I_x & & \\ & \mathrm{d}I_y & \\ & & \mathrm{d}I_z\end{bmatrix}$ is the matrix composed of moments of inertia of the micro-segment $\mathrm{d}x$.

$$\begin{cases}\mathrm{d}I_x=\dfrac{\rho A_k(x)\left(l_y^2+l_z^2\right)}{12}\mathrm{d}x,\\ \mathrm{d}I_y=\dfrac{\rho l_y l_z^3}{12}\mathrm{d}x,\\ \mathrm{d}I_z=\dfrac{\rho l_y^3 l_z}{12}\mathrm{d}x.\end{cases} \quad (16)$$

In summary, the kinetic energy of the element is

$$T_k=\frac{1}{2}\begin{bmatrix}\boldsymbol{u}_i^{\mathrm{T}} & \boldsymbol{u}_j^{\mathrm{T}}\end{bmatrix}\boldsymbol{M}_k\begin{bmatrix}\boldsymbol{u}_i\\ \boldsymbol{u}_j\end{bmatrix}, \quad (17)$$

where $\boldsymbol{M}_k=\int_0^{l_k}\rho\overline{\boldsymbol{N}}_{k1}^{\mathrm{T}}A_k(x)\overline{\boldsymbol{N}}_{k1}\mathrm{d}x+\int_0^{l_k}\boldsymbol{N}_{k2}^{\mathrm{T}}\mathrm{d}\boldsymbol{I}\overline{\boldsymbol{N}}_{k2}$ is the mass matrix of the element.

The elastic potential energy of the element can be expressed as

$$V_k^e=\frac{1}{2}\begin{bmatrix}\boldsymbol{u}_i^{\mathrm{T}} & \boldsymbol{u}_j^{\mathrm{T}}\end{bmatrix}\boldsymbol{K}_k\begin{bmatrix}\boldsymbol{u}_i\\ \boldsymbol{u}_j\end{bmatrix}, \quad (18)$$

where $\boldsymbol{K}_k=\begin{bmatrix}-\boldsymbol{D}_k^{\mathrm{T}}(j)\\ \boldsymbol{E}\end{bmatrix}\boldsymbol{k}_k\begin{bmatrix}-\boldsymbol{D}_k(j) & \boldsymbol{E}\end{bmatrix}$ is the stiffness matrix of the element.

Using the assembly method in the finite element method, the mass matrix and stiffness matrix of the substructure can be obtained.

$$\boldsymbol{M}_c=\sum\boldsymbol{P}_{ck}^{\mathrm{T}}\boldsymbol{R}_{ck}^{\mathrm{T}}\boldsymbol{M}_{ck}\boldsymbol{R}_{ck}\boldsymbol{P}_{ck}, \quad (19)$$

$$\boldsymbol{K}_c=\sum\boldsymbol{P}_{ck}^{\mathrm{T}}\boldsymbol{R}_{ck}^{\mathrm{T}}\boldsymbol{K}_{ck}\boldsymbol{R}_{ck}\boldsymbol{P}_{ck}, \quad (20)$$

where $\boldsymbol{R}_{ck}$ is the transformation matrix from global coordinate to local coordinate. $\boldsymbol{P}_{ck}$ is a matrix composed of 0 and 1, which represents the position of the element in the global frame.

3.2 Mass Matrix and Stiffness Matrix of Each Substructure

According to the structural characteristics of the RPR type compliant parallel mechanism, its branches are divided into several sub-structures. In view of the similarity of the two types of branches, only one of them is analyzed in the paper.

Taking the RPU branch as an example, the branch is split into three sub-structures, namely a flexible R pair, a U pair and a displacement amplifier. They are denoted as A, B, and C respectively, as shown in Figure 5. In substructure C, the flexible leaf spring is a single beam element, and the other connecting beams are divided into three beam elements with the same length. Consequently, substructure C is split into 26 beam elements (including 26 nodes). The nodes c_1 and c_{14} are connected to the R pair and the U pair, respectively.

In substructure C, each element is not connected end to end, but offset. The connection of elements c_4c_5, c_5c_6 and c_6c_7 is shown in Figure 6. The actual nodes of the leaf spring element are c_5^* and c_6^*. c_5^* and c_5 are not directly connected, but there is a deviation d_e. Assume that there is a rigid and massless linkage $c_5c_5^*$ connecting two

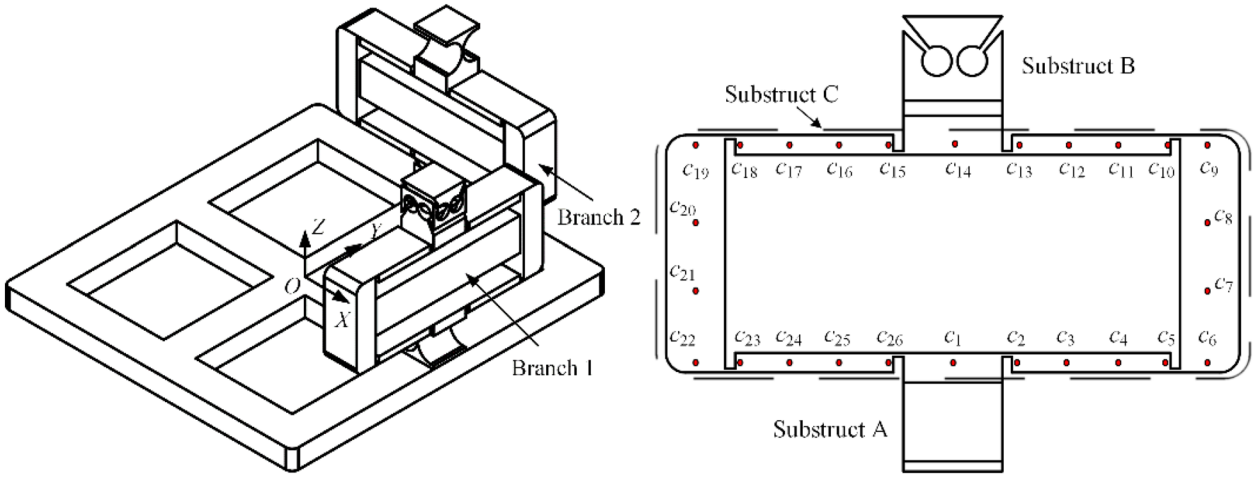

Figure 5 Schematic diagram of compliant mechanism and its discretization

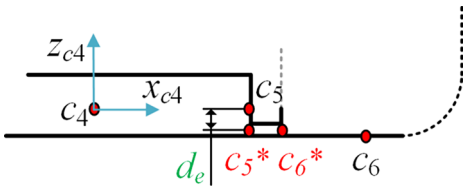

Figure 6 Sketch of the element deviation in the displacement amplifier

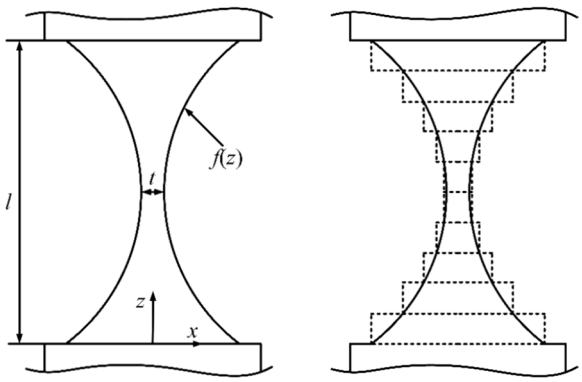

Figure 7 Sketch of the simplified U pair and its discretization

Table 2 Size parameters of beam elements in Substructure C

	Length (mm)	Width (mm)	Height (mm)
c_1c_2 element	1	10	0.4
c_2c_3 element	5	10	2
c_6c_7 element	8	10	6

adjacent elements, thus the displacement and force relationship of nodes c_5* and c_5 can be expressed as

$$\boldsymbol{u}_{c_5*} = \boldsymbol{D}_e^1 \boldsymbol{u}_{c_5}, \tag{21}$$

$$\boldsymbol{f}_{c_4*} = \boldsymbol{D}_e^2 \boldsymbol{f}_{c_4}, \tag{22}$$

where

$$\boldsymbol{D}_e^1 = \begin{bmatrix} \boldsymbol{r}_5 & \boldsymbol{r}_5\hat{\boldsymbol{d}}_e \\ \boldsymbol{0} & \boldsymbol{r}_5 \end{bmatrix}, \tag{23}$$

$$\boldsymbol{D}_e^2 = -\begin{bmatrix} \boldsymbol{r}_5 & \boldsymbol{0} \\ \boldsymbol{r}_5\hat{\boldsymbol{d}}_e & \boldsymbol{r}_5 \end{bmatrix}, \tag{24}$$

$\boldsymbol{u}_{c_5*}$ and $\boldsymbol{u}_{c_5}$ are displacements of c_5* and c_5, respectively. $\boldsymbol{f}_{c_4*}$ and $\boldsymbol{f}_{c_4}$ are node forces of c_5* and c_5, respectively. $\boldsymbol{r}_5$ is coordinate transformation matrix from coordinate of c_4c_5 to this of c_5c_6. $\hat{\boldsymbol{d}}_e$ is the skew-symmetric matrix defined by the translational vector $\boldsymbol{d}_e$.

There are three sizes of beam elements, and their size parameters are shown in Table 2. The mass matrix and stiffness matrix of the C substructure can be obtained by substituting the parameters in Table 2 into Eqs. (19)–(22).

Since the structure of the flexible U pair is relatively complicated, it is simplified here as a notched U pair. The xy view is shown in Figure 7, and its parameters l and t are consistent with the structural parameters of the original U pair. The contour line of the simplified U pair is part of an ellipse, and its equation $f(z)$ is shown in Table 3.

Table 3 The contour line of the simplified U pair

The simplified U pair	$f(z)=-b\sqrt{1-\frac{(x-a-t)^2}{a^2}}+b\ (x>0)$ $f(z)=b\sqrt{1-\frac{(z+a+t)^2}{a^2}}-b\ (x<0)$	$a=\frac{10-t}{2}$ mm	$b=5$ mm

Substructures A and B are beams with variable cross-sections. When calculating their compliance matrices and mass matrices, they are approximately discretized into 10 uniform beam elements with the same length, as shown in Figure 7. The mass matrix and stiffness matrix of the beam element in substructures A and B can be obtained by substituting the parameters in Table 3 into Eqs. (19) and (20).

4 Dynamic Modeling of the RPR Type Mechanism with Low Orders

After obtaining the stiffness matrix and mass matrix of all substructures, the dynamic modeling with low orders of the whole mechanism is built based on the C-B method.

4.1 Truncated Modes of Each Substructure

Substructures A and B are composed of 10 beam elements with different sections in series. One end of substructure A is fixed, and the other end is the boundary. Both ends of B are boundaries. The degree of freedom of each boundary node is equal to 6. Therefore, the constrained modes of substructures A and B can be expressed as

$$[\boldsymbol{\psi}_A]^{\lambda}=\begin{bmatrix}\boldsymbol{\psi}_c^A\\ \boldsymbol{I}_{6\times 6}\end{bmatrix}, \tag{25}$$

$$[\boldsymbol{\psi}_B]^{\lambda}=\begin{bmatrix}\boldsymbol{I}_{6\times 6} & \boldsymbol{0}\\ \boldsymbol{\psi}_c^B & \overline{\boldsymbol{\psi}}_c^B\\ \boldsymbol{0} & \boldsymbol{I}_{6\times 6}\end{bmatrix}, \tag{26}$$

where $\boldsymbol{I}_{6\times 6}$ is an identity matrix. $\boldsymbol{\psi}_c^A$,$\boldsymbol{\psi}_c^B$ and $\overline{\boldsymbol{\psi}}_c^B$ can be obtained by Eq. (6).

The nodes c_1 and c_{14} are boundaries of substructure C, and their constraint modes can be recorded as

$$\left[\boldsymbol{\psi}_C\right]^{\lambda}=\begin{bmatrix}\boldsymbol{I}_{6\times 6} & \boldsymbol{0}_{6\times 6}\\ {}_{7:84}\boldsymbol{\psi}_{c1}^C & {}_{7:84}\overline{\boldsymbol{\psi}}_{c1}^C\\ \boldsymbol{0}_{6\times 6} & \boldsymbol{I}_{6\times 6}\\ {}_{91:162}\boldsymbol{\psi}_{c2}^C & {}_{91:162}\overline{\boldsymbol{\psi}}_{c2}^C\end{bmatrix}. \tag{27}$$

The solution of $\left[\boldsymbol{\psi}_C\right]^{\lambda}$ is as follows: Firstly, a new matrix is formed by removing the 85th–90th rows and the 85th–90th columns of the stiffness matrix of C after fixing c_{14}. The first 6 columns in Eq. (27) can be obtained by substituting the new matrix into Eq. (6). Secondly, a new matrix is formed by removing the first six rows and columns of the stiffness matrix C after fixing c_1. The last six columns in Eq. (27) can be obtained by substituting the new matrix into Eq. (6).

4.2 The First Coordinate Transformation

The first coordinate transformation in the modal synthesis method is to transform the physical coordinates into modal coordinates, to obtain the principal mass matrix and principal stiffness matrix of each substructure. Notably, the orders of the principal mass matrix and the principal stiffness matrix are equal to the coordination number of the truncated mode.

$$\begin{cases}\boldsymbol{M}_A^{\lambda}=\left\{[\boldsymbol{\psi}_A]^{\lambda}\right\}^{\mathrm{T}}\boldsymbol{M}_A[\boldsymbol{\psi}_A]^{\lambda},\\ \boldsymbol{M}_B^{\lambda}=\left\{[\boldsymbol{\psi}_B]^{\lambda}\right\}^{\mathrm{T}}\boldsymbol{M}_B[\boldsymbol{\psi}_B]^{\lambda},\\ \boldsymbol{M}_C^{\lambda}=\left\{\left[\boldsymbol{\psi}_C\right]^{\lambda}\right\}^{\mathrm{T}}\boldsymbol{M}_C\left[\boldsymbol{\psi}_C\right]^{\lambda},\end{cases} \tag{28}$$

$$\begin{cases}\boldsymbol{K}_A^{\lambda}=\left\{[\boldsymbol{\psi}_A]^{\lambda}\right\}^{\mathrm{T}}\boldsymbol{K}_A[\boldsymbol{\psi}_A]^{\lambda},\\ \boldsymbol{K}_B^{\lambda}=\left\{[\boldsymbol{\psi}_B]^{\lambda}\right\}^{\mathrm{T}}\boldsymbol{K}_B[\boldsymbol{\psi}_B]^{\lambda},\\ \boldsymbol{K}_C^{\lambda}=\left\{\left[\boldsymbol{\psi}_C\right]^{\lambda}\right\}^{\mathrm{T}}\boldsymbol{K}_C\left[\boldsymbol{\psi}_C\right]^{\lambda}.\end{cases} \tag{29}$$

Let $\overline{\boldsymbol{M}}=\begin{bmatrix}\boldsymbol{M}_A & & \\ & \boldsymbol{M}_C & \\ & & \boldsymbol{M}_B\end{bmatrix}$ and $\overline{\boldsymbol{K}}=\begin{bmatrix}\boldsymbol{K}_A & & \\ & \boldsymbol{K}_C & \\ & & \boldsymbol{K}_B\end{bmatrix}$ be the principal mass matrix and the principal stiffness matrix of the branch, respectively.

4.3 Second Coordinate Transformation

The second coordinate transformation in the modal synthesis method is to remove the non-independent coordinates and retain the independent coordinates in each substructure. It is not difficult to find that the coordinates of the nodes connecting the two substructures are non-independent. Let ${}^{Lim}\boldsymbol{p}=\left[\boldsymbol{p}_C^{\mathrm{T}}\ \boldsymbol{p}_{B2}^{\mathrm{T}}\right]^{\mathrm{T}}$ be a set of independent modal coordinates. $\boldsymbol{p}_C$ is the modal coordinate of substructure C. $\boldsymbol{p}_{B2}$ is the last 6 elements of $\boldsymbol{p}_B$, and $\boldsymbol{p}_B$ is the modal coordinate of substructure B. The following relationship can be obtained

$$\begin{bmatrix} \boldsymbol{p}_A \\ \boldsymbol{p}_C \\ \boldsymbol{p}_B \end{bmatrix} = \overline{\boldsymbol{T}}^{Lim} \boldsymbol{p}, \tag{30}$$

where $\overline{\boldsymbol{T}}^{Lim} = \begin{bmatrix} \overline{\boldsymbol{T}}_1 \\ \overline{\boldsymbol{T}}_2 \\ \overline{\boldsymbol{T}}_3 \end{bmatrix}$, $\overline{\boldsymbol{T}}_1 = \begin{bmatrix} \boldsymbol{I}_{6\times6} & \boldsymbol{0}_{6\times12} \end{bmatrix}$, $\overline{\boldsymbol{T}}_2 = [\boldsymbol{I}_{12\times12}$ $\boldsymbol{0}_{6\times6}]$, $\overline{\boldsymbol{T}}_3 = \begin{bmatrix} \boldsymbol{0}_{6\times6} & \boldsymbol{I}_{12\times12} \end{bmatrix}$.

4.4 Dynamic Equation of the Whole Mechanism

The moving platform is regarded as an ideal rigid body. The relationship between the physical coordinate and modal coordinate of the node connected to the moving platform in substructure B is

$$\boldsymbol{u}_{B2} = \boldsymbol{p}_{B2}. \tag{31}$$

The relationship between the coordinates of the center of the moving platform and $\boldsymbol{u}_{B2}$ is

$$\boldsymbol{u}_{B2} = \boldsymbol{D}_{mp}\boldsymbol{u}_s, \tag{32}$$

where $\boldsymbol{u}_s$ is the coordinate of the center of the moving platform. $\boldsymbol{D}_{mp} = \begin{bmatrix} \boldsymbol{r}_{mp} & \boldsymbol{r}\hat{\boldsymbol{d}}_{mp} \\ \boldsymbol{0} & \boldsymbol{r}_{mp} \end{bmatrix}$ is the adjoint transformation matrix.

The independent coordinates of the whole mechanism can be expressed as $\boldsymbol{p} = \begin{bmatrix} {}^{Lim1}\overline{\boldsymbol{p}}^{\mathrm{T}} & {}^{Lim2}\overline{\boldsymbol{p}}^{\mathrm{T}} & {}^{Lim3}\overline{\boldsymbol{p}}^{\mathrm{T}} & {}^{Lim4}\overline{\boldsymbol{p}}^{\mathrm{T}} & \boldsymbol{u}_s \end{bmatrix}^{\mathrm{T}}$, where ${}^{Limi}\overline{\boldsymbol{p}}(i = 1, 2, 3, 4)$ is a new modal coordinate formed by removing $\boldsymbol{p}_{B2}$ in ${}^{Limi}\boldsymbol{p}$. The relationship between the generalized coordinate of the whole mechanism and that of each branch is

$$\begin{bmatrix} {}^{Lim1}\boldsymbol{p} \\ {}^{Lim2}\boldsymbol{p} \\ {}^{Lim3}\boldsymbol{p} \\ {}^{Lim4}\boldsymbol{p} \end{bmatrix} = \begin{bmatrix} {}^{Lim1}\boldsymbol{T} \\ {}^{Lim2}\boldsymbol{T} \\ {}^{Lim3}\boldsymbol{T} \\ {}^{Lim4}\boldsymbol{T} \end{bmatrix} \boldsymbol{p}, \tag{33}$$

where ${}^{Lim1}\boldsymbol{T} = \begin{bmatrix} \boldsymbol{R}_{s1} & \boldsymbol{0} & \boldsymbol{0} & \boldsymbol{0} & \boldsymbol{0} \\ \boldsymbol{0} & \boldsymbol{0} & \boldsymbol{0} & \boldsymbol{0} & \boldsymbol{D}_1 \end{bmatrix}$,

$${}^{Lim2}\boldsymbol{T} = \begin{bmatrix} \boldsymbol{0} & \boldsymbol{R}_{s2} & \boldsymbol{0} & \boldsymbol{0} & \boldsymbol{0} \\ \boldsymbol{0} & \boldsymbol{0} & \boldsymbol{0} & \boldsymbol{0} & \boldsymbol{D}_2 \end{bmatrix},$$

$${}^{Lim3}\boldsymbol{T} = \begin{bmatrix} \boldsymbol{0} & \boldsymbol{0} & \boldsymbol{R}_{s3} & \boldsymbol{0} & \boldsymbol{0} \\ \boldsymbol{0} & \boldsymbol{0} & \boldsymbol{0} & \boldsymbol{0} & \boldsymbol{D}_3 \end{bmatrix},$$

$${}^{Lim4}\boldsymbol{T} = \begin{bmatrix} \boldsymbol{0} & \boldsymbol{0} & \boldsymbol{0} & \boldsymbol{R}_{s4} & \boldsymbol{0} \\ \boldsymbol{0} & \boldsymbol{0} & \boldsymbol{0} & \boldsymbol{0} & \boldsymbol{D}_4 \end{bmatrix}.$$

$\boldsymbol{R}_{si}$ $(i = 1, 2, 3, 4)$ is the coordinate transformation matrix from the global frame to the branch frame.

The overall mass matrix and stiffness matrix of the mechanism are

$$\boldsymbol{M} = \sum {}^{Limj}\boldsymbol{T}^{\mathrm{T}}\overline{\boldsymbol{T}}^{\mathrm{T}}\overline{\boldsymbol{M}}\,\overline{\boldsymbol{T}}\boldsymbol{T}^{Limj} + \boldsymbol{T}_s^{\mathrm{T}}\boldsymbol{M}_s\boldsymbol{T}_s, \tag{34}$$

$$\boldsymbol{K} = \sum {}^{Limj}\boldsymbol{T}^{\mathrm{T}}\overline{\boldsymbol{T}}^{\mathrm{T}}\overline{\boldsymbol{K}}\,\overline{\boldsymbol{T}}\boldsymbol{T}^{Limj}, \tag{35}$$

where $\boldsymbol{T}_s = \begin{bmatrix} \boldsymbol{0} & \boldsymbol{0} & \boldsymbol{0} & \boldsymbol{0} & \boldsymbol{I} \end{bmatrix}$.

The free vibration model of the RPR type mechanism without damping can be expressed as

$$\boldsymbol{M}\ddot{\boldsymbol{p}} + \boldsymbol{K}\boldsymbol{p} = \boldsymbol{0}. \tag{36}$$

The natural frequency of the RPR type mechanism can be obtained by

$$\left|\boldsymbol{K} - \omega^2\boldsymbol{M}\right| = 0. \tag{37}$$

According to the retained modes, we can know the order of the mass matrix and the stiffness matrix in Eq. (36) is only 54, which is much smaller than the original order of the system.

5 Dynamic Simulation of RPR Type Compliant Parallel Mechanism

In this section, Ansys Workbench is used to conduct modal simulations to verify the established dynamic model of the RPR type mechanism. In addition, the material selection is Al-7075.

The first 6-order modes obtained by simulation are shown in Figure 8. Due to the out-of-plan deformation of the displacement amplifier, undesired motions of the moving platform are expressed in the first 3 modes. The last three modes are the working modes of the RPR type mechanism, namely 2R1T. When the actuator is installed in the motion amplifier, the out-of-plane deformation would be suppressed. Subsequently, the defective movement of the moving platform will be eliminated.

The modal synthesis method is an approximate dynamic modeling method. In addition, the simplified processing of the flexible hinge also introduces unavoidable errors. It can be seen in Table 4 that the maximum error is not more than 15% between the theoretical analysis and the simulation results. As the cost of improving solution efficiency, a larger error is totally acceptable. Especially, when the modeling of the flexible hinge is more accurate, the overall dynamics of the mechanism will be more accurate.

6 Experiment and Analysis

A dynamic experiment is conducted to obtain the dynamic characteristics of the RPR type compliant mechanism. The amplifier and flexible hinges in each branch are fabricated by wire electrical discharge machining, and the whole body is assembled by screws (Figure 9).

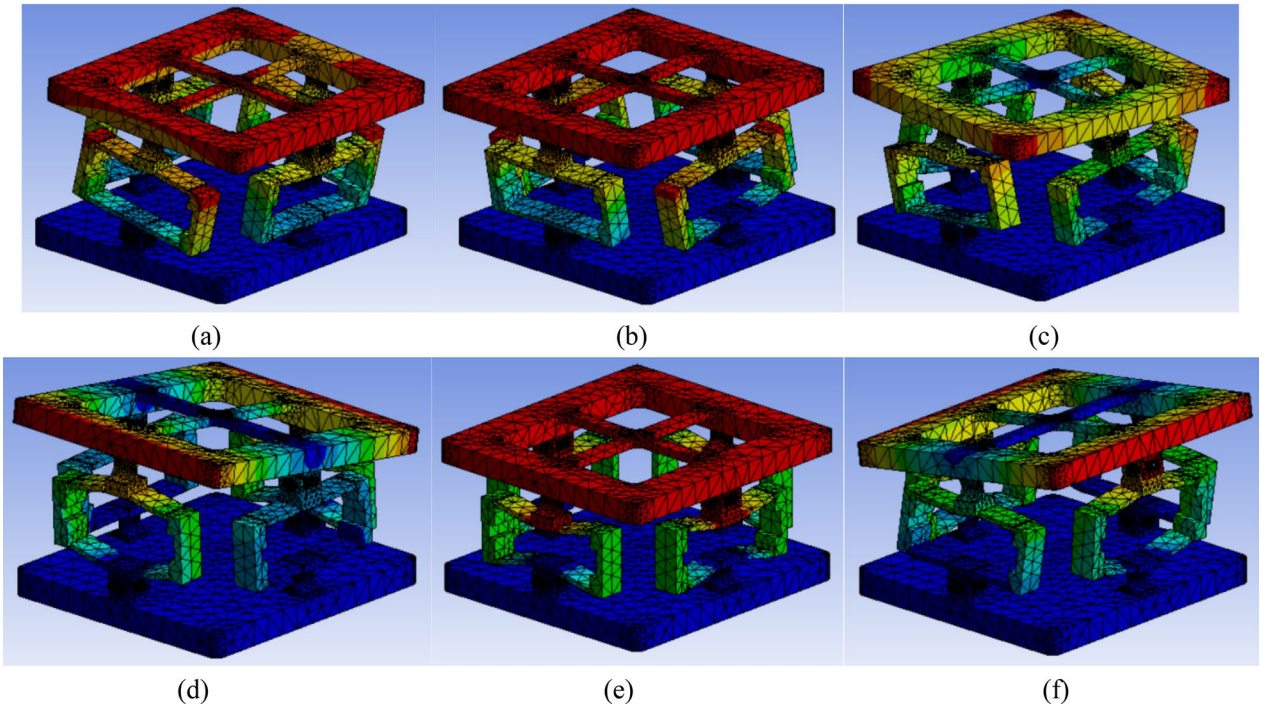

Figure 8 The modal simulation results of the mechanism, (**a**)–(**f**) are the first 6 mode shapes

Table 4 The first 6 natural frequencies of the RPR type mechanism obtained by theoretical analysis and simulation analysis (rad/s)

	1st mode	2nd mode	3rd mode	4th mode	5th mode	6th mode
Simulation	51.297	59.227	85.449	127.24	135.36	144.15
Theoretical analysis	46.23	54.86	75.65	141.56	153.73	165.27
Relative errors	9.88%	7.37%	11.47%	11.25%	13.57%	14.65%

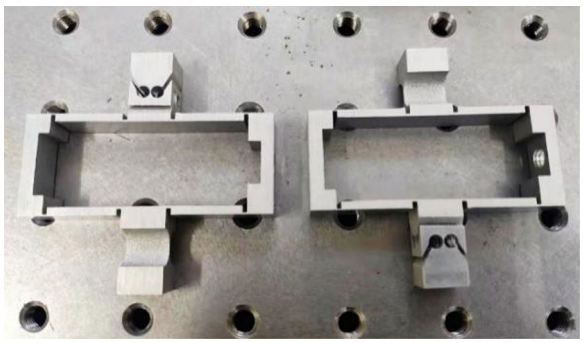

Figure 9 Two kinds of branches

A modal hammer is utilized to provide impulse force on the output stage to excite vibration. Two acceleration sensors (LW369802 from PCB PIEZOTRONICS, Inc.) are used to measure the vibration response of the moving platform. A vibration and noise analyzer (SCM2E05 from Siemens, Inc.) is utilized to analyze the vibration signal from the acceleration sensors.

The sensors are mounted on the moving platform in four ways to measure the dynamic response of the moving platform in 6 DoFs, as shown in Figure 10. The dynamic experiment is divided into four steps according to the placement of the sensor. In each step, the impact points are hit successively by the modal hammer. The vibration signal from sensors is collected and processed by the vibration and noise analyzer. To avoid randomness, each step of the experiment is carried out five times. The result takes the average of the values obtained from the five experiments.

The curves of the frequency response functions (FRFs) obtained by the vibration and noise analyzer are given in Figure 11. And the resonance frequencies of the first-six orders obtained from the experiment are listed in Table 5. The resonance frequencies obtained by analytical model, simulation and experiment are relatively close. In addition, the natural frequencies obtained by the experiment are slightly smaller than those obtained by simulation.

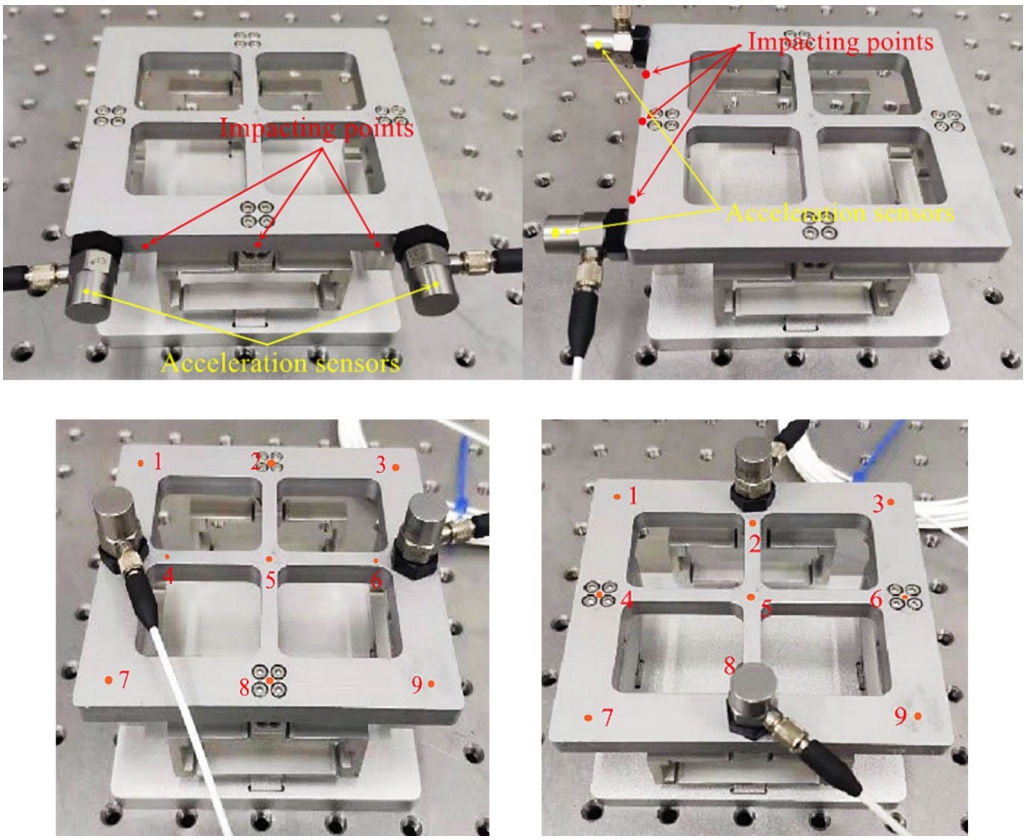

Figure 10 Placements of sensors and corresponding knocking points

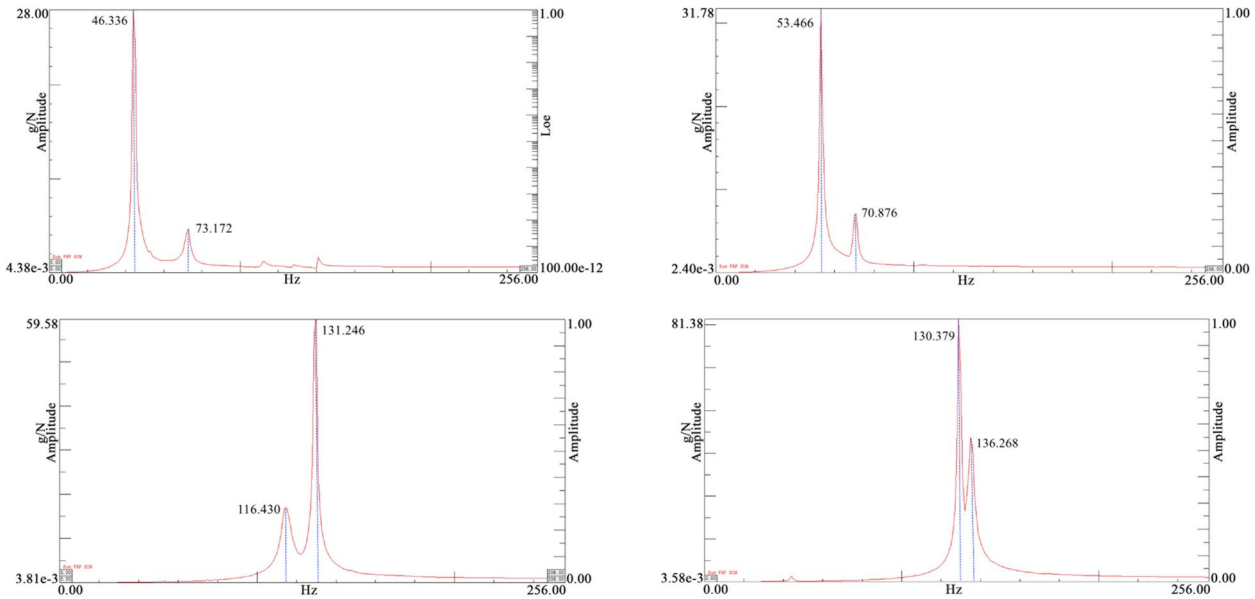

Figure 11 The frequency response functions obtained by the vibration and noise analyzer

Table 5 The first 6 natural frequencies of the RPR type mechanism obtained by the experiment (rad/s)

1st mode	2nd mode	3rd mode	4th mode	5th mode	6th mode
46.861	53.470	75.364	115.270	129.333	133.536

The lower frequency is due to the increase in mass of the moving platform caused by the contact sensors.

7 Conclusions

A dynamic model with low orders of an RPR type compliant parallel mechanism is established based on the distributed parameter method and a modified modal synthesis method. The RPR type compliant parallel mechanism has two vertical continuous rotation axes relative to the fixed coordinate, which are known. Based on the elastic beam model, the stiffness matrix and mass matrix of connecting beams and flexible hinges are established considering the moment of inertia. The modified modal synthesis method is used to reduce the order of the dynamic equation of the mechanism. The order of the whole dynamic equation is only 54, which greatly reduces time consumption of the space spring mass system with 173 nodes. The dynamic modeling method used in the paper belongs to substructure technology. The obtained dynamic model not only simplifies the calculation of dynamic characteristics of the complex mechanism, but also simplifies the calculation of the dynamic response. Furthermore, the dynamic model is verified by finite element simulation. The relative errors of the natural frequencies obtained by theoretical analysis and simulation are less than 15%. The simplification of the flexure hinge results in lower accuracy. Finally, a dynamic experiment is conducted to obtain the dynamic characteristics of the mechanism. The experimental result shows that the resonance frequencies obtained by the developed dynamic model are correct. And the resonance frequencies of the developed mechanism are slightly smaller than those obtained by finite element simulation, which verifies the effectiveness of the established dynamic equation. The dynamic model with low orders established in the paper has higher computational efficiency and also meets the accuracy requirements. This model will provide effective assistance for practical application of the mechanism. And the dynamic response and control of the RPR type mechanism will be studied in the future based on the dynamic model.

Acknowledgements
Not applicable.

Author Contributions
SZ was responsible for the main content of the manuscript, including theoretical analysis and calculation, as well as writing. JL was in charge of the whole trivia. HD assisted with theoretical analysis and article writing. YZ put forward constructive suggestions. All authors read and approved the final manuscript.

Funding
Supported by National Natural Science Foundation of China (Grant No. 51975007).

Data availability
The datasets generated during and/or analyzed during the current study are available from the corresponding author on reasonable request.

Declarations

Competing Interests
The authors declare no competing financial interests.

Received: 18 October 2022 Revised: 19 May 2024 Accepted: 28 May 2024
Published online: 25 July 2024

References

[1] H M F Vatan, M Hamedi. Design, analysis and fabrication of a novel hybrid electrothermal microgripper in micro-assembly cell. *Micro-electronic Engineering*, 2020, 6: 111374.
[2] M N M Zubir, B Shirinzadeh, Y Tian. A new design of piezoelectric driven compliant-based microgripper for micromanipulation. *Mechanism and Machine Theory*, 2015, 44(12): 2248-2264.
[3] Y He, P Zou, Z Zhu, et al. Design and application of a flexure-based oscillation mechanism for surface texturing. *Journal of Manufacturing Processes*, 2018, 32: 298-306.
[4] Z Zhu, S To, K F Ehmann, et Al. Design, analysis, and realization of a novel piezoelectrically actuated rotary spatial vibration system for micro-/nanomachining. *IEEE-ASME Transactions on Mechatronics*, 2017, 22(3): 1227-1237.
[5] X Zhou, R Wang, Q Liu, et Al. Development of a 2-degree-of-freedom decoupled flexural mechanism for micro/nanomachining. *Proceedings of the Institution of Mechanical Engineers, Part B: Journal of Engineering Manufacture*, 2014, 229(11): 1900-1911.
[6] B J Kenton, K K Leang. Design and control of a three-axis serial-kinematic high-bandwidth nano-positioner. *IEEE-ASME Transactions on Mechatronics*, 2012, 17(2): 356-369.
[7] N He, W Jia, M Gong, et al. Design and mechanism analysis of a novel type compact single mirror laser scanner. *Sensors and Actuators A: Physical*, 2016, 125(2): 482-485.
[8] H S Kim, Y M Cho. Design and modeling of a novel 3-DOF precision micro-stage. *Mechatronics*, 2009, 19(5): 598-608.
[9] J H Park, H S Lee. Design of a piezoelectric-driven tilt mirror for a fast laser scanner. *Japanese Journal of Applied Physics*, 2012, 51(9): 1-14.
[10] H Kim, J Kim, D Ahn, et al. Development of a nano-precision 3-DOF vertical positioning system with a flexure hinge. *IEEE Transactions on Nanotechnology*, 2013, 12(2): 234-245.
[11] G B Hao, X He. Designing a monolithic tip-tilt-piston flexure manipulator. *Archives of Civil and Mechanical Engineering*, 2017, 17(4): 871-879.
[12] J Yu, S Bi, G Zong, et al. On the design of compliant-based micro-motion manipulators with a nanometer range resolution. *Proceedings 2003 IEEE/ASME International Conference on Advanced Intelligent Mechatronics (AIM 2003)*, Kobe, Japan, 2003: 149-154.
[13] S Zhang, J F Liu, H F Ding, et al. A novel compliance modeling method for compliant parallel mechanisms and its application. *Mechanism and Machine Theory*, 2021, 162: 104336.
[14] Y Q Yu, S K Zhu, Q P Xu, et al. A novel model of large deflection beams with combined end loads in compliant mechanisms. *Precision Engineering*, 2016, 43: 395-405.
[15] Y Q Yu, P Zhou, Q P Xu. Kinematic and dynamic analysis of compliant mechanisms considering both lateral and axial deformations of flexural beams. *Proceedings of the Institution of Mechanical Engineers, Part C: Journal of Mechanical Engineering Science*, 2019, 233(3): 1-14.

[16] X Pei, J J Yu, G H Zong, et al. An effective pseudo-rigid-body method for beam-based compliant mechanisms. *Precision Engineering*, 2010, 34(3): 634-639.
[17] H. Tang, Y. M. Li. Development and active disturbance rejection control of a compliant micro-/nano-positioning piezostage with dual mode. *IEEE Transactions on Industrial Electronics*, 2014, 61(3): 1475-1492.
[18] X Zhu, X Xu, Z Wen, et al. A novel flexure-based vertical nano-positioning stage with large travel range. *Review of Scientific Instruments*, 2015, 86(10): 105112.
[19] Y Shen, X Chen, W Jiang, et al. Spatial force-based non-prismatic beam element for static and dynamic analyses of circular flexure hinges in compliant mechanisms. *Precision Engineering*, 2014, 38(2): 311-320.
[20] J W Ryu, S Q Lee, D G Gweon, et al. Inverse kinematic modeling of a coupled flexure hinge mechanism. *Mechatronics*, 1999, 9(6): 657-674.
[21] W Zhu, X T Rui. Modeling of a three degrees of freedom piezo-actuated mechanism. *Smart Materials and Structures*, 2017, 26(1): 015006.
[22] M X Ling, J Y Cao, N Pehrson. Kinetostatic and dynamic analyses of planar compliant mechanisms with a two-port dynamic stiffness model. *Precision Engineering*, 2019, 57: 149-161.
[23] M X Ling, L L Howell, J Y Cao, et al. A pseudo-static model for dynamic analysis on frequency domain of distributed compliant mechanisms. *Journal of Mechanisms and Robotics*, 2018, 10(5): 051011.
[24] M X Ling. A general two-port dynamic stiffness model and static/dynamic comparison for three bridge-type flexure displacement. *Mechanical Systems and Signal Processing*, 2019, 119: 486-500.
[25] M X Ling, S L Chen, Q S Li, et al. Dynamic stiffness matrix for free vibration analysis of flexure hinges based on non-uniform Timoshenko beam. *Journal of Sound and Vibration*, 2018, 437: 40-52.
[26] M X Ling, S D Z Song, et al. Analysis and design of spatial compliant mechanisms using a 3-D dynamic stiffness model. *Mechanism and Machine Theory*, 2022, 168: 104581.
[27] Shao D, Wang Q, Y Tao, et al. A unified thermal vibration and transient analysis for quasi-3D shear deformation composite laminated beams with general boundary conditions. *International Journal of Mechanical Sciences*, 2021, 198: 106357.
[28] G Gao, N Sun, D Shao, et al. A unified analysis for the free vibration of the sandwich piezoelectric laminated beam with general boundary conditions under the thermal environment. *Shock and Vibration*, 2021: 1-21.
[29] J F Doyle. Wave Propagation in structures. New York: Springer-Verlag, 1989.
[30] R Craig, M Bampton. Coupling of substructures for dynamic analysis. *AIAA Journal*, 1968, 6(7): 1313-1319.
[31] W C Hurty. Vibrations of structural systems by component mode synthesis. *Journal of the Engineering Mechanics Division*, 1960, 86: 51-69.

Shuang Zhang born in 1991, received his Ph.D. degree in mechanical engineering from *Beijing University of Technology, China*, in 2022. His research interests include compliant mechanisms, and parallel mechanisms.

Jingfang Liu born in 1985, is currently a professor at *Beijing University of Technology, China*. She received her Ph.D. degree in mechanical engineering from *Yanshan University, China*, in 2011. Her research interests include compliant mechanisms, and parallel mechanisms.

Huafeng Ding born in 1977, is currently a professor at *Beijing University of Technology, China*. He received the first Ph.D. degree in mechanical engineering from *Yanshan University, China,* in 2007, and the second Ph.D. degree in mechanical engineering from *the University of Duisburg-Essen, Germany*, in 2015. His current research interests include parallel mechanisms and hybrid mechanisms, etc.

Yanbin Zhang born in 1974, is currently a professor at *Henan University of Science and Technology, China*. He received his Ph.D. degree in mechanical engineering from *Xi'an University of Technology, China*, in 2008. His current research interests include parallel mechanisms, and rehabilitation robots.